Molecular Physics, Vol. 104, No. 4, 20 February 2006, 571–586

Taylor & Francis
Taylor & Francis Group

On the thermodynamics of diblock chain fluids from simulation and heteronuclear statistical associating fluid theory for potentials of variable range

YUN PENG, HONGGANG ZHAO and CLARE McCABE*
Department of Chemical Engineering, Vanderbilt University, Nashville, TN 37235-1604, USA

(*Received 1 September 2005*)

The SAFT-VR equation of state is extended to treat heteronuclear chain fluids, focusing, in particular, on symmetric and asymmetric diblock chains. The chain molecules studied are composed of segments of different size and/or energy of interaction. Both symmetric and asymmetric systems are considered. The theoretical predictions are compared with isothermal–isobaric and Gibbs ensemble Monte Carlo simulation data. Excellent agreement is obtained between the hetero-SAFT-VR predictions and the simulation data, validating the use of the SAFT-VR approach for heteronuclear chains in more realistic models of polymers and small molecules composed of different functional groups.

Keywords: SAFT-VR; Heteronuclear; Diblock; Chain fluids; Simulation

1. Introduction

Predicting the thermodynamic properties of chain fluids, such as hydrocarbons and polymers, has attracted considerable interest in recent years. To this end, numerous equations of state have been proposed in the literature to describe the thermodynamics and phase behaviour of chain molecules and their mixtures [1, 2]. The most successful of these, in terms of their predictive capabilities, are rooted in statistical mechanics and provide an accurate, molecular-based approach. Molecular-based equations of state (EOSs), such as those derived from the SAFT approach [3, 4], provide a framework in which the effects of molecular shape and interactions on the thermodynamic properties can be separated and quantified. The explicit description of the molecular level interactions enables the parameters of the resulting equation of state to have physical meaning, leading to more predictive capabilities and a limited reliance on fitting to experimental data. For example, using different variations of the SAFT equation, several authors have shown for the n-alkane homologous series that the molecular parameters which characterize the length of the model chain, the size of the segments and the magnitude of their interaction, behave smoothly with molecular weight [5–13].

*Corresponding author. Email: c.mccabe@vanderbilt.edu

An important feature of the SAFT equation of state is that it explicitly takes into account the non-sphericity and association interactions of real molecules. In the SAFT formalism, following the seminal work of Wertheim [14–17], the free energy is written as the sum of four separate contributions:

$$\frac{A}{NkT} = \frac{A^{\text{ideal}}}{NkT} + \frac{A^{\text{mono}}}{NkT} + \frac{A^{\text{chain}}}{NkT} + \frac{A^{\text{assoc}}}{NkT}, \qquad (1)$$

where N is the number of molecules, k Boltzmann's constant, and T the temperature. A^{ideal} is the ideal free energy, A^{mono} the contribution to the free energy due to the monomer segments, A^{chain} the contribution due to the formation of bonds between monomer segments, and A^{assoc} is the contribution due to association. Hence, a SAFT fluid is a collection of monomers that can form covalent bonds; the monomers interact via repulsive and attractive (dispersion) forces, and, in some cases, association interactions. Since the SAFT EOS has a firm basis in statistical mechanical perturbation theory for well-defined molecular models, systematic improvement (e.g., by improved expressions for the monomer free energy and structure) and extension of the theory (e.g., by considering new monomer fluids, bonding schemes and association interactions) is possible by comparing the theoretical predictions with computer simulation results on the same molecular model. This advantage over empirical EOSs has resulted in many

Molecular Physics
ISSN 0026–8976 print/ISSN 1362–3028 online © 2006 Taylor & Francis
http://www.tandf.co.uk/journals
DOI: 10.1080/00268970500475901

extensions and variations of the original SAFT expressions (for details the reader is referred to the excellent reviews by Economou [3] and Muller and Gubbins [4]). The many different versions of SAFT essentially correspond to different choices for the monomer fluid, and different theoretical approaches to the calculation of the monomer free energy and structure. In this work we focus on SAFT-VR, which describes chain molecules formed from hard-core monomers with attractive potentials of variable range (SAFT-VR) [18, 19], typically a square well. In this version of the theory the dispersive interactions are treated via a second-order high-temperature perturbation expansion providing a more rigorous description of the thermodynamics than found in simpler versions of the SAFT approach [20]. SAFT-VR has been successfully used to describe the phase equilibria of a wide range of industrially important systems and provides significant improvement and predictive capability over earlier formulations. For example, alkanes of low molecular weight through to simple polymers [9, 20–24], and their binary mixtures [21, 25–30], perfluoroalkanes [31, 32], hydrogen fluoride [33], water [34], refrigerant systems [35], carbon dioxide [29, 36–39], and electrolyte solutions [40–42] have all been studied.

In recent years, heteronuclear versions of SAFT which allow the model chain to be composed of segments of different size and/or energy have been proposed by several authors [5, 43–53]. One of the first applications of hetero-SAFT to chain fluids focused on hard systems and compared the theoretical predictions of PVT behaviour with simulation data for block, alternate and random copolymers [46]. The SAFT predictions were shown to be more accurate than the available equations of state for heteronuclear chain fluids [54–57], performing well over a range of densities. Of particular interest is the work of Radosz and co-workers on copolymer SAFT [44], which allows for the description of linear and branched copolymers within Wertheim's first-order thermodynamic perturbation theory. In this approach, molecules composed of two distinct types of segments are considered and the sequence of segments is described through segment and bonding fractions. Copolymer SAFT was initially applied to the engineering version of SAFT proposed by Huang and Radosz [58] to model real copolymer systems [44, 59], and later to Lennard–Jones [60] and square-well-based SAFT models [5, 61]. Heteronuclear Lennard–Jones chains have also been studied by Tang [62] and Blas and Vega [45]; in both cases the thermodynamics of heteronuclear dimers were studied. More recently, Sadowski and co-workers have proposed PC-SAFT [63], which has been shown to be successful in modelling polymer systems [49, 64] and has been extended to hetero-segmented molecules [49, 50] using the bond and segment fraction approach suggested by Banaszak *et al.* [44].

In this work we extend the SAFT-VR approach to study hetero-segmented chain fluids, as a move towards more realistic models of polymers and small molecules composed of different functional groups. A heteronuclear version of the SAFT-VR equation of state was applied in earlier work to dimer fluids and excellent agreement was obtained between simulation data and theoretical predictions for the PVT behaviour of the systems studied [48]. Here we extend the hetero-SAFT-VR approach to chain fluids and rigorously test the predictions against both PVT and phase equilibrium simulation data. The theoretical predictions are compared to isothermal–isobaric (*NPT*) and Gibbs ensemble Monte Carlo (GEMC) simulations of symmetric and asymmetric diblock chain molecules. The remainder of the paper is organized as follows. In section 2 the hetero-SAFT-VR approach and molecular models studied are presented. In section 3 details of the simulations performed are given, the results of which are compared to the theoretical predictions in section 4. Finally, conclusions are drawn and future work discussed in section 5.

2. Hetero-SAFT-VR approach

In the SAFT-VR approach, chain molecules are formed from tangentially bonded monomer segments that interact through an attractive potential of variable range. Specifically, each segment interacts through a square well (SW) potential,

$$U_{ij}(r) = \begin{cases} +\infty & \text{if } r < \sigma_{ij}, \\ -\varepsilon_{ij} & \text{if } \sigma_{ij} \le r < \lambda_{ij}\sigma_{ij}, \\ 0 & \text{if } r \ge \lambda_{ij}\sigma_{ij}, \end{cases} \tag{2}$$

where σ_{ij} is the diameter of the interaction, λ_{ij} the range and ε_{ij} the well depth of the SW potential. In the original SAFT-VR approach, applicable to homonuclear chains, all of the segments have the same σ, λ and ε. In this work the chains are composed of segments of different size and/or energy. The inter- and intra-molecular cross interactions between segments are obtained from the Lorentz–Berthelot combining rules [65],

$$\sigma_{ij} = \frac{\sigma_{ii} + \sigma_{jj}}{2}, \tag{3}$$

$$\varepsilon_{ij} = \sqrt{\varepsilon_{ii}\varepsilon_{jj}}, \tag{4}$$

$$\lambda_{ij} = \frac{\lambda_{ii}\sigma_{ii} + \lambda_{jj}\sigma_{jj}}{\sigma_{ii} + \sigma_{jj}}. \tag{5}$$

Table 1. Potential model parameters for the symmetric and asymmetric diblock chain fluids studied. m_1 and m_2 are the number of segments of type 1 and type 2, respectively. σ_2/σ_1 is the ratio of the hard core diameter of segments of type 2 to type 1. $\varepsilon_2/\varepsilon_1$ the ratio of the depth of the attractive interaction between segments of type 2 and type 1. λ the range of the potential.

System	m_2	m_1	σ_2/σ_1	$\varepsilon_2/\varepsilon_1$	λ
1	2	2	1	1.5	1.5
2	2	2	1	0.5	1.5
3	2	2	2	1.5	1.5
4	2	2	2	1.0	1.5
5	2	2	2	0.5	1.5
6	2	2	2	1.0	1.4
7	2	2	2	1.0	1.6
8	4	4	1	1.5	1.5
9	4	4	1	0.5	1.5
10	4	4	2	1.5	1.5
11	4	4	2	1.0	1.5
12	4	4	2	0.5	1.5
13	2	4	2	1.5	1.5
14	2	4	2	1.0	1.5
15	2	4	2	0.5	1.5
16	2	6	2	1.5	1.5
17	2	6	2	1.0	1.5
18	2	6	2	0.5	1.5

A total of 18 diblock fluids have been studied over a range of state conditions with chain lengths of $m=4$, 6, and 8. For each system the diblock chains are composed of segments with different size and/or different energy of interaction. The details of each system studied are given in table 1.

The general form of the Helmholtz free energy A within the SAFT framework is given by equation (1). We will present each contribution in turn for the treatment of pure fluids composed of polyatomic heteronuclear molecules followed by the specific equations needed to describe diblock chains. We do not give details of the association term since the chain fluids considered in this work are non-associating.

The ideal contribution to the free energy is expressed as

$$\frac{A^{\text{ideal}}}{NkT} = \ln(\rho\Lambda^3) - 1, \tag{6}$$

where N is the total number of molecules, k Boltzmann's constant, ρ the number density of chain molecules and Λ the thermal de Broglie wavelength.

The monomer free energy is given by

$$\frac{A^{\text{mono}}}{NkT} = m\frac{A^{\text{M}}}{N_{\text{s}}kT} = ma^{\text{M}}, \tag{7}$$

where N_{s} is the total number of segments, determined from the product of the total number of molecules N and the number of segments per molecule m. a^{M} is free energy per monomer segment and in the SAFT-VR equation is approximated by a second-order high-temperature expansion using Barker and Henderson perturbation theory for mixtures [66], viz.

$$a^{\text{M}} = a^{\text{HS}} + \beta a_1 + \beta^2 a_2, \tag{8}$$

where $\beta = 1/kT$, a^{HS} is the free energy of the hard sphere reference fluid and a_1 and a_2 are the first and second perturbation terms, respectively.

The hard sphere reference term a^{HS} is determined from the expression of Boublik [67] and Mansoori and co-workers [68] for multi-component hard sphere systems, viz.

$$a^{\text{HS}} = \frac{6}{\pi\rho_{\text{s}}}\left[\left(\frac{\zeta_2^3}{\zeta_3^2} - \zeta_0\right)\ln(1-\zeta_3) + \frac{3\zeta_1\zeta_2}{1-\zeta_3} + \frac{\zeta_2^3}{\zeta_3(1-\zeta_3)^2}\right], \tag{9}$$

where ρ_{s} is the number density of segments, which is defined as N_{s}/V, the total number of segments divided by the total volume, and ζ_l is the reduced density given by a sum over all segments types i,

$$\begin{aligned}\zeta_l &= \frac{\pi}{6}\rho_{\text{s}}\left[\sum_{i=1}^{n} x_{\text{s},i}(\sigma_i)^l\right] \\ &= \frac{\pi}{6}\rho_{\text{s}}[x_{\text{s},1}(\sigma_1)^l + x_{\text{s},2}(\sigma_2)^l],\end{aligned} \tag{10}$$

where σ_i is the diameter of segments of type i and $x_{\text{s},i}$ is the mole fraction of segments of type i. Note that ζ_3 is the volume fraction occupied by the molecules and is generally denoted η.

The first perturbation term a_1 describing the mean-attractive energy is obtained from the sum of all pair interactions,

$$\begin{aligned}a_1 &= \sum_{i=1}^{n}\sum_{j=1}^{n} x_{\text{s},i}x_{\text{s},j}(a_1)_{ij} \\ &= x_{\text{s},1}^2(a_1)_{11} + 2x_{\text{s},1}x_{\text{s},2}(a_1)_{12} + x_{\text{s},2}^2(a_1)_{22},\end{aligned} \tag{11}$$

where $(a_1)_{ij}$ is obtained from the mean-value theorem as proposed by Gil-Villegas *et al.* [18],

$$\begin{aligned}(a_1)_{ij} &= -2\pi\rho_{\text{s}}\varepsilon_{ij}\int_{\sigma_{ij}}^{\infty} r_{ij}^2 g_{ij}^{\text{HS}}(r_{ij})\text{d}r_{ij} \\ &= -\rho_{\text{s}}\alpha_{ij}^{\text{VDW}} g_{ij}^{\text{HS}}(\sigma_{ij};\zeta_3^{\text{eff}}),\end{aligned} \tag{12}$$

where

$$\alpha_{ij}^{\text{VDW}} = \frac{2\pi}{3}\sigma_{ij}^3\varepsilon_{ij}(\lambda_{ij}^3 - 1). \tag{13}$$

Within the Van der Waals one fluid theory the radial distribution function $g_{ij}^{\mathrm{HS}}(\sigma_{ij}; \zeta_3^{\mathrm{eff}})$ is approximated by that for a pure fluid, hence equation (12) becomes

$$(a_1)_{ij} = -\rho_s \alpha_{ij}^{\mathrm{VDW}} g_0^{\mathrm{HS}}[\sigma_x; \zeta_x^{\mathrm{eff}}(\lambda_{ij})], \tag{14}$$

where $g_0^{\mathrm{HS}}(\sigma_x; \zeta_x^{\mathrm{eff}})$ is obtained from the Carnahan and Starling equation of state [69],

$$g_0^{\mathrm{HS}}[\sigma_x; \zeta_x^{\mathrm{eff}}(\lambda_{ij})] = \frac{1 - \zeta_x^{\mathrm{eff}}/2}{(1 - \zeta_x^{\mathrm{eff}})^3}. \tag{15}$$

The effective packing fraction $\zeta_x^{\mathrm{eff}}(\lambda_{ij})$ is obtained within the Van der Waals one fluid theory from the corresponding packing fraction of the mixture ζ_x given by

$$\zeta_x^{\mathrm{eff}}(\zeta_x, \lambda_{ij}) = c_1(\lambda_{ij})\zeta_x + c_2(\lambda_{ij})\zeta_x^2 + c_3(\lambda_{ij})\zeta_x^3, \tag{16}$$

where

$$\begin{pmatrix} c_1 \\ c_2 \\ c_3 \end{pmatrix} = \begin{pmatrix} 2.25855 & -1.50349 & 0.249434 \\ -0.669270 & 1.40049 & -0.827739 \\ 10.1576 & -15.0427 & 5.30827 \end{pmatrix} \begin{pmatrix} 1 \\ \lambda_{ij} \\ \lambda_{ij}^2 \end{pmatrix}, \tag{17}$$

and

$$\zeta_x = \frac{\pi}{6}\rho_s \sigma_x^3, \tag{18}$$

with

$$\begin{aligned} \sigma_x^3 &= \sum_{i=1}^{n}\sum_{j=1}^{n} x_{s,i} x_{s,j} \sigma_{ij}^3 \\ &= x_{s,1}^2 \sigma_{11}^3 + 2x_{s,1}x_{s,2}\sigma_{12}^3 + x_{s,2}^2 \sigma_{22}^3. \end{aligned} \tag{19}$$

This corresponds to mixing rule MX1b in the original SAFT-VR approach for mixtures [19]. We have compared the results obtained from this formulation with the MX3b mixing rule [19], in which the actual packing fraction of the system is used to obtain ζ_3^{eff}, and found that the difference between the two was negligible in most cases. Therefore, despite the more rigorous nature of the MX3b approach, we chose MX1b in order to avoid convergence problems in the critical region of the phase diagram [19, 21].

The second-order perturbation term for the monomer excess free energy a_2 is expressed as

$$\begin{aligned} a_2 &= \sum_{i=1}^{n}\sum_{j=1}^{n} x_{s,i} x_{s,j} (a_2)_{ij} \\ &= x_{s,1}^2 (a_2)_{11} + 2x_{s,1}x_{s,2}(a_2)_{12} + x_{s,2}^2 (a_2)_{22}, \end{aligned} \tag{20}$$

where $(a_2)_{ij}$ is obtained through the local compressibility approximation:

$$(a_2)_{ij} = \frac{1}{2} K^{\mathrm{HS}} \varepsilon_{ij} \rho_s \frac{\partial (a_1)_{ij}}{\partial \rho_s}, \tag{21}$$

and K^{HS} is the Percus–Yevick expression for the hard-sphere isothermal compressibility,

$$K^{\mathrm{HS}} = \frac{\zeta_0 (1 - \zeta_3)^4}{\zeta_0 (1 - \zeta_3)^2 + 6\zeta_1\zeta_2(1 - \zeta_3) + 9\zeta_2^3}. \tag{22}$$

Finally, the contribution due to chain formation from the monomer segments is given in terms of the background correlation function y_{ij}^{SW},

$$\frac{A^{\mathrm{chain}}}{NkT} = -\sum_{ij\,\mathrm{bonds}} \ln y_{ij}^{\mathrm{SW}}(\sigma_{ij}), \tag{23}$$

where the sum is over all bonds in the chain molecule,

$$y_{ij}^{\mathrm{SW}}(\sigma_{ij}) = \exp(-\beta\varepsilon_{ij}) g_{ij}^{\mathrm{SW}}(\sigma_{ij}). \tag{24}$$

For the diblock systems studied in this work, equation (23) becomes

$$\begin{aligned} \frac{A^{\mathrm{chain}}}{NkT} = &-(m_1 - 1)\ln y_{11}^{\mathrm{SW}}(\sigma_{11}) - \ln y_{12}^{\mathrm{SW}}(\sigma_{12}) \\ &- (m_2 - 1)\ln y_{22}^{\mathrm{SW}}(\sigma_{22}). \end{aligned} \tag{25}$$

The radial distribution function for the square well monomers $g_{ij}^{\mathrm{SW}}(\sigma_{ij})$ is approximated by a first-order high-temperature perturbation expansion:

$$g_{ij}^{\mathrm{SW}}(\sigma_{ij}; \zeta_3) = g_{ij}^{\mathrm{HS}}(\sigma_{ij}; \zeta_3) + \beta\varepsilon_{ij} g_1^{\mathrm{SW}}(\sigma_{ij}), \tag{26}$$

where the contact value of the radial distribution function $g_{ij}^{\mathrm{HS}}(\sigma_{ij}; \zeta_3)$ at the actual packing fraction ζ_3 is obtained from the expression of Boublik [67],

$$g_{ij}^{\mathrm{HS}}(\sigma_{ij}; \zeta_3) = \frac{1}{1 - \zeta_3} + 3\frac{D_{ij}\zeta_3}{(1 - \zeta_3)^2} + 2\frac{(D_{ij}\zeta_3)^2}{(1 - \zeta_3)^3}, \tag{27}$$

where

$$\begin{aligned} D_{ij} &= \frac{\sigma_{ii}\sigma_{jj}\sum_{i=1}^{n} x_{s,i}\sigma_{ii}^2}{(\sigma_{ii} + \sigma_{jj})\sum_{i=1}^{n} x_{s,i}\sigma_{ii}^3} \\ &= \frac{\sigma_{ii}\sigma_{jj}(x_{s,1}\sigma_{11}^2 + x_{s,2}\sigma_{22}^2)}{(\sigma_{ii} + \sigma_{jj})(x_{s,1}\sigma_{11}^3 + x_{s,2}\sigma_{22}^3)}, \end{aligned} \tag{28}$$

and $g_1^{SW}(\sigma_{ij})$ is determined using the Clausius virial theorem and the first derivative of the free energy with respect to the density [18], giving

$$g_1^{SW}(\sigma_{ij}) = \frac{1}{2\pi\varepsilon_{ij}\sigma_{ij}^3}\left[3\left(\frac{\partial(a_1)_{ij}}{\partial\rho_s}\right) - \frac{\lambda_{ij}}{\rho_s}\frac{\partial(a_1)_{ij}}{\partial\lambda_{ij}}\right]. \quad (29)$$

In order to determine the thermodynamics and phase equilibria for each model fluid studied the pressure and chemical potential can be calculated from the Helmholtz free energy through standard thermodynamic relationships:

$$\mu = \left(\frac{\partial A}{\partial N}\right)_{T,V}, \quad (30)$$

$$P = -\left(\frac{\partial A}{\partial V}\right)_{T,N}. \quad (31)$$

3. Simulation details

We have performed Monte Carlo (MC) simulations to determine the *PVT* and phase behaviour of 18 model diblock chain fluids (listed in table 1) to compare with the theoretical predictions and test the accuracy of the hetero-SAFT-VR approach for diblock chains.

Isothermal–isobaric (*NPT*) MC simulations have been performed for each fluid studied at several state conditions to ensure a wide range of temperatures and pressures are examined. Initial configurations were generated by placing molecules on a face centred cubic lattice; simulations at higher pressure, and hence density, were started from this equilibrated configuration and allowed to re-equilibrate to the corresponding density. The simulations were performed with $N = 128$ molecules for all fluids. The usual periodic boundary conditions and minimum image convention were applied. In order to test the *NPT* MC code developed for heteronuclear chain fluids, comparisons were made, and agreement achieved, between the results obtained in this work and the work of Gulati and Hall [70], who studied symmetric square-well diblock 4-mer, 8-mer, and 16-mer chains at a single reduced temperature using continuous canonical molecular dynamics.

GEMC simulations have also been performed for selected fluids to determine the fluid phase diagram. The initial configurations for each simulation were taken from equilibrated *NPT* runs at either densities approximately midway between those for the liquid and vapour phase at each state condition or close to the corresponding theoretical solutions. Simulations were performed with $N = 256$ molecules. As for the *NPT* simulations the usual periodic boundary conditions and minimum image convention were applied.

In both the *NPT* and GEMC simulations, one cycle consisted of N attempted MC moves (chosen randomly from displacement and reorientation), one volume change and a specified number of attempted re-growths (*NPT*) or insertions (GEMC) of randomly selected molecules using continuum configurational bias sampling [71]. The maximum displacement and volume changes were adjusted to give an acceptance ratio of between 30 and 40%. The number of attempted re-growths/insertions was controlled so that between 1 and 3% of the molecules was re-grown or inserted each cycle. The thermodynamic properties of the system were obtained as ensemble averages and the errors estimated by determining the standard deviation. An initial simulation of 50 000–250 000 cycles was performed to equilibrate the system, depending upon pressure and chain length, before averaging for between 250 000 and 1 000 000 cycles.

4. Results

In all, twelve symmetric and six asymmetric diblock chain fluids have been studied; systems 1–7 are symmetric diblock 4-mer fluids, systems 8–12 symmetric diblock 8-mer fluids, systems 13–15 asymmetric diblock 6-mer fluids, and systems 16–18 asymmetric diblock 8-mer fluids. For each chain length we consider molecules in which: the segments are of the same size but have different well depths (systems 1, 2, 8, and 9); the segments are of different sizes but have the same well depth (systems 4, 6, 7, 11, 14 and 17); the segments have different sizes and different values of the well depth (systems 3, 5, 10, 12, 13, 15, 16 and 18). The details of each system are given in table 1. For each system we have studied isotherms at reduced temperatures of $T^* = 2$, 3, 4, and 5, where $T^* = kT/\varepsilon_1$. The hetero-SAFT-VR EOS predictions are compared against *NPT* MC (reported in tables 2–5) and GEMC simulation data (given in tables 6 and 7).

In figure 1 we present the isotherms studied for the diblock 4-mer fluids (systems 1 and 2) composed of segments with equal diameters ($\sigma_2 = \sigma_1$), a potential range of $\lambda_1 = \lambda_2 = 1.5$, and different well depths $\varepsilon_2 \neq \varepsilon_1$. From the figure we see that system 1 (figure 1*a*), which has a higher ratio of $\varepsilon_2/\varepsilon_1 = 1.5$ than system 2 (figure 1*b*), displays higher densities at a given pressure. We observe good agreement between the simulation results and theoretical predictions over a wide range of temperatures and pressures. In contrast,

Table 2. *NPT* MC simulation results for the symmetric diblock 4-mer fluids studied (systems 1–7). The reduced temperature is given by $T^* = kT/\varepsilon_1$, the pressure as $P^* = P\sigma_1^3/\varepsilon_1$, and the energy is defined per segment as $E^* = E/N_s\varepsilon_1$.

System	T^*	P^*	η	E^*	System	T^*	P^*	η	E^*
1	2	2.2134	0.402 ± 0.005	-5.97 ± 0.09	4	4	0.5633	0.304 ± 0.007	-2.99 ± 0.09
	3	0.2327	0.172 ± 0.012	-2.40 ± 0.16			1.8327	0.401 ± 0.005	-4.23 ± 0.08
		1.0840	0.298 ± 0.007	-4.04 ± 0.13		5	0.2691	0.204 ± 0.008	-1.84 ± 0.09
		5.8699	0.402 ± 0.005	-5.81 ± 0.10			0.8170	0.304 ± 0.006	-2.93 ± 0.09
	4	0.6761	0.194 ± 0.008	-2.43 ± 0.12			2.5078	0.401 ± 0.005	-4.19 ± 0.08
		2.4281	0.299 ± 0.006	-3.95 ± 0.12	5	2	0.0767	0.211 ± 0.010	-1.33 ± 0.07
		9.5555	0.402 ± 0.005	-5.72 ± 0.09			0.2340	0.308 ± 0.007	-1.97 ± 0.06
	5	1.1220	0.199 ± 0.008	-2.39 ± 0.12			0.8091	0.402 ± 0.005	-2.71 ± 0.05
		3.7827	0.301 ± 0.006	-3.91 ± 0.11		3	0.1633	0.206 ± 0.008	-1.18 ± 0.06
		13.2528	0.402 ± 0.005	-5.68 ± 0.09			0.4866	0.304 ± 0.007	-1.85 ± 0.06
2	2	0.2417	0.188 ± 0.009	-1.47 ± 0.08			1.4836	0.402 ± 0.005	-2.64 ± 0.05
		0.9536	0.298 ± 0.007	-2.36 ± 0.07		4	0.2499	0.205 ± 0.007	-1.13 ± 0.05
		4.3166	0.402 ± 0.005	-3.40 ± 0.06			0.7408	0.304 ± 0.006	-1.80 ± 0.05
	3	0.6868	0.200 ± 0.008	-1.42 ± 0.07			2.1597	0.402 ± 0.005	-2.59 ± 0.05
		2.3051	0.300 ± 0.006	-2.29 ± 0.06		5	0.3367	0.205 ± 0.007	-1.10 ± 0.05
		8.0106	0.401 ± 0.005	-3.34 ± 0.05			0.9957	0.303 ± 0.006	-1.77 ± 0.05
	4	1.1342	0.201 ± 0.007	-1.37 ± 0.06			2.8364	0.401 ± 0.004	-2.57 ± 0.05
		3.6660	0.302 ± 0.006	-2.27 ± 0.07	6	2	0.0472	0.211 ± 0.013	-1.77 ± 0.11
		11.7152	0.401 ± 0.004	-3.30 ± 0.05			0.1466	0.312 ± 0.009	-2.59 ± 0.10
	5	1.5824	0.202 ± 0.006	-1.34 ± 0.06			0.5894	0.406 ± 0.006	-3.60 ± 0.08
		5.0308	0.302 ± 0.006	-2.25 ± 0.06		3	0.1346	0.207 ± 0.009	-1.51 ± 0.08
		15.4240	0.401 ± 0.004	-3.29 ± 0.05			0.3971	0.307 ± 0.007	-2.37 ± 0.08
3	2	0.2050	0.404 ± 0.006	-6.17 ± 0.11			1.2584	0.404 ± 0.005	-3.44 ± 0.07
	3	0.0343	0.192 ± 0.017	-2.89 ± 0.21		4	0.2218	0.205 ± 0.008	-1.41 ± 0.07
		0.1528	0.308 ± 0.009	-4.35 ± 0.16			0.6503	0.305 ± 0.007	-2.28 ± 0.08
		0.8660	0.402 ± 0.005	-5.93 ± 0.10			1.9318	0.402 ± 0.005	-3.37 ± 0.07
	4	0.1204	0.203 ± 0.010	-2.71 ± 0.14		5	0.3088	0.204 ± 0.007	-1.35 ± 0.07
		0.4022	0.306 ± 0.008	-4.15 ± 0.14			0.9045	0.305 ± 0.006	-2.23 ± 0.07
		1.5353	0.401 ± 0.005	-5.78 ± 0.10			2.6070	0.402 ± 0.005	-3.34 ± 0.07
	5	0.2068	0.205 ± 0.009	-2.59 ± 0.13	7	2	0.3987	0.402 ± 0.005	-5.46 ± 0.08
		0.6542	0.305 ± 0.007	-4.04 ± 0.13		3	0.0546	0.206 ± 0.013	-2.72 ± 0.16
		2.2080	0.401 ± 0.005	-5.72 ± 0.10			0.2266	0.307 ± 0.008	-3.95 ± 0.12
4	2	0.0099	0.119 ± 0.039	-1.75 ± 0.33			1.0668	0.401 ± 0.005	-5.28 ± 0.08
		0.0625	0.307 ± 0.011	-3.31 ± 0.13		4	0.1404	0.206 ± 0.010	-2.53 ± 0.13
		0.4905	0.403 ± 0.005	-4.46 ± 0.08			0.4783	0.305 ± 0.007	-3.80 ± 0.11
	3	0.0960	0.206 ± 0.010	-2.05 ± 0.11			1.7398	0.401 ± 0.005	-5.20 ± 0.08
		0.3111	0.306 ± 0.007	-3.09 ± 0.10		5	0.2266	0.205 ± 0.008	-2.42 ± 0.11
		1.1594	0.402 ± 0.005	-4.31 ± 0.08			0.7316	0.304 ± 0.006	-3.74 ± 0.10
	4	0.1825	0.206 ± 0.008	-1.92 ± 0.10			2.4147	0.401 ± 0.005	-5.16 ± 0.08

figure 2 presents isotherms for diblock 4-mer fluids (systems 3–5) composed of segments with a size ratio of $\sigma_2/\sigma_1 = 2$, a potential range of $\lambda_1 = \lambda_2 = 1.5$ and differing well depths. System 3 in figure 2(*a*) has the highest ratio of interaction energies, $\varepsilon_2/\varepsilon_1 = 1.5$, and system 5 (figure 2*c*) the lowest, $\varepsilon_2/\varepsilon_1 = 0.5$. We again observe that the system with the higher ratio of well depths is denser at a given pressure, however in comparison to system 1, system 3 has much larger densities under the same pressures due to size effects. Similar behaviour is expected and observed for system 5 compared to system 2. Again, in all cases, excellent agreement is observed between the theoretical predictions and the simulation data.

To test the effect of the range of the potential on the *PVT* and phase behaviour, in figure 3 we also present results for 4-mer fluids that have the same size ratio ($\sigma_2/\sigma_1 = 2$) and equal well depth ($\varepsilon_2 = \varepsilon_1$), but different potential range ($\lambda_1 = \lambda_2 = 1.6$ and $\lambda_1 = \lambda_2 = 1.4$). From the figure we can see that system 7, which has the

Table 3. *NPT* MC simulation results for the symmetric diblock 8-mer fluids studied (systems 8–12). See table 2 for details.

System	T^*	P^*	η	E^*	System	T^*	P^*	η	E^*
8	2	1.6202	0.395 ± 0.004	-5.60 ± 0.10	11	2	0.0028	0.296 ± 0.012	-3.18 ± 0.11
	3	0.0360	0.088 ± 0.031	-1.73 ± 0.29			0.3728	0.399 ± 0.004	-4.26 ± 0.06
		0.6444	0.295 ± 0.005	-3.86 ± 0.09		3	0.0514	0.202 ± 0.009	-2.02 ± 0.09
		5.0170	0.400 ± 0.005	-5.57 ± 0.11			0.2186	0.309 ± 0.006	-3.01 ± 0.08
	4	0.4009	0.266 ± 0.009	-3.48 ± 0.12			0.9855	0.401 ± 0.004	-4.14 ± 0.06
		1.8370	0.300 ± 0.005	-3.81 ± 0.08		4	0.1208	0.206 ± 0.007	-1.88 ± 0.07
		8.4412	0.399 ± 0.004	-5.46 ± 0.10			0.4381	0.307 ± 0.005	-2.88 ± 0.07
	5	0.7684	0.199 ± 0.006	-2.33 ± 0.09			1.6025	0.402 ± 0.003	-4.09 ± 0.05
		3.0404	0.302 ± 0.004	-3.76 ± 0.08		5	0.1904	0.208 ± 0.007	-1.82 ± 0.07
		11.8767	0.399 ± 0.004	-5.42 ± 0.07			0.6591	0.306 ± 0.005	-2.82 ± 0.07
9	2	0.1089	0.176 ± 0.010	-1.42 ± 0.07			2.2213	0.401 ± 0.003	-4.05 ± 0.05
		0.6600	0.297 ± 0.005	-2.28 ± 0.05	12	2	0.0480	0.215 ± 0.009	-1.42 ± 0.06
		3.7508	0.397 ± 0.004	-3.24 ± 0.05			0.1739	0.309 ± 0.005	-1.98 ± 0.05
	3	0.4755	0.200 ± 0.006	-1.39 ± 0.05			0.6924	0.401 ± 0.003	-2.65 ± 0.03
		1.8601	0.302 ± 0.004	-2.22 ± 0.04		3	0.1176	0.211 ± 0.006	-1.23 ± 0.04
		7.1833	0.399 ± 0.003	-3.20 ± 0.04			0.3937	0.308 ± 0.005	-1.85 ± 0.04
	4	0.8446	0.203 ± 0.005	-1.34 ± 0.05			1.3106	0.401 ± 0.003	-2.58 ± 0.03
		3.0698	0.303 ± 0.004	-2.19 ± 0.05		4	0.1872	0.210 ± 0.006	-1.16 ± 0.04
		10.6258	0.398 ± 0.003	-3.17 ± 0.04			0.6152	0.307 ± 0.004	-1.79 ± 0.04
	5	1.2145	0.204 ± 0.005	-1.31 ± 0.04			1.9304	0.401 ± 0.003	-2.54 ± 0.03
		4.2834	0.303 ± 0.004	-2.17 ± 0.04		5	0.2570	0.208 ± 0.005	-1.11 ± 0.04
		14.0724	0.398 ± 0.003	-3.15 ± 0.04			0.8373	0.305 ± 0.005	-1.74 ± 0.04
10	2	0.0858	0.396 ± 0.003	-5.73 ± 0.07			2.5509	0.400 ± 0.003	-2.52 ± 0.03
	3	0.0613	0.303 ± 0.008	-4.11 ± 0.12					
		0.6906	0.401 ± 0.003	-5.63 ± 0.07					
	4	0.0603	0.195 ± 0.010	-2.57 ± 0.12					
		0.2779	0.306 ± 0.006	-3.95 ± 0.10					
		1.3037	0.399 ± 0.003	-5.49 ± 0.06					
	5	0.1296	0.203 ± 0.007	-2.48 ± 0.10					
		0.4972	0.307 ± 0.005	-3.86 ± 0.09					
		1.9201	0.400 ± 0.003	-5.44 ± 0.06					

greatest potential range ($\lambda = 1.6$), exhibits a higher density at a given pressure compared to system 6, which has a shorter potential range ($\lambda = 1.4$).

If we consider longer chain lengths, the isotherms for 8-mer fluids are presented in figures 4 and 5. Similar trends are seen in the isotherms as a function of the size ratio and interaction energy for the 8-mer systems as for the 4-mer fluids. Again, excellent agreement is in general observed between the theoretical predictions and the simulation data, though slight deviations are seen at low densities for the systems studied in figure 4. We can also note from the figures that, at a given pressure, the densities for the 8-mer fluids are slightly higher than those observed for the corresponding 4-mer systems due to chain length effects.

To examine the effect of symmetry on the isotherms we have studied a number of asymmetric 6-mer (systems 13–15) and 8-mer fluids (systems 16–18), the results of which are presented in figures 6 and 7, respectively. For each chain length, each system studied has the same asymmetric molecular structure with $\sigma_2/\sigma_1 = 2$, a potential range of $\lambda_1 = \lambda_2 = 1.5$ but different ratios of the well depths ($\varepsilon_2/\varepsilon_1$). Good agreement is observed between the theory and simulation for each system studied. We also note from the figures that increasing the fraction of the smaller segments (m_1) within a molecule results in lower densities at a given pressure. For example, the asymmetric 8-mer fluids (systems 16–18) have a higher fraction of small segments than the symmetric 8-mer fluids (systems 10–12), and therefore lower densities at a given pressure (comparing systems with the same ratio of $\varepsilon_2/\varepsilon_1$). Similarly, if we consider the asymmetric 6-mer fluids (systems 13–15), which have a lower fraction of small segments than the asymmetric 8-mer fluids (systems 16–18), for the same ratio of $\varepsilon_2/\varepsilon_1$ the asymmetric 6-mer systems have higher densities at a given pressure than the corresponding asymmetric 8-mer systems, despite having less segments per molecule.

Table 4. *NPT* MC simulation results for the asymmetric diblock 6-mer (systems 13–15) and 8-mer (systems 16–18) fluids studied. See table 2 for details.

System	T^*	P^*	η	E^*	System	T^*	P^*	η	E^*
13	2	0.2135	0.405 ± 0.004	-5.65 ± 0.08	16	2	0.2443	0.398 ± 0.004	-5.24 ± 0.07
	3	0.0249	0.181 ± 0.018	-2.62 ± 0.18		3	0.0183	0.196 ± 0.012	-2.63 ± 0.12
		0.1611	0.311 ± 0.008	-4.00 ± 0.12			0.1745	0.307 ± 0.007	-3.73 ± 0.10
		1.0170	0.405 ± 0.005	-5.44 ± 0.08			1.1804	0.401 ± 0.004	-5.11 ± 0.06
	4	0.1231	0.205 ± 0.009	-2.52 ± 0.12		4	0.1275	0.206 ± 0.008	-2.41 ± 0.10
		0.4569	0.307 ± 0.007	-3.79 ± 0.11			0.5132	0.310 ± 0.006	-3.62 ± 0.09
		1.8309	0.404 ± 0.005	-5.31 ± 0.08			2.1280	0.400 ± 0.004	-5.00 ± 0.06
	5	0.2215	0.206 ± 0.008	-2.40 ± 0.11		5	0.2370	0.208 ± 0.008	-2.30 ± 0.09
		0.7557	0.307 ± 0.006	-3.69 ± 0.10			0.8554	0.307 ± 0.005	-3.49 ± 0.08
		2.6488	0.404 ± 0.004	-5.24 ± 0.08			3.0803	0.401 ± 0.003	-4.97 ± 0.06
14	2	0.0315	0.311 ± 0.009	-3.33 ± 0.10	17	2	0.0048	0.312 ± 0.009	-3.32 ± 0.08
		0.5088	0.405 ± 0.005	-4.36 ± 0.07			0.5408	0.402 ± 0.004	-4.28 ± 0.06
	3	0.0898	0.209 ± 0.009	-2.09 ± 0.09		3	0.0844	0.211 ± 0.009	-2.11 ± 0.09
		0.3252	0.309 ± 0.007	-3.05 ± 0.09			0.3403	0.308 ± 0.006	-2.99 ± 0.08
		1.3208	0.404 ± 0.004	-4.20 ± 0.07			1.4853	0.403 ± 0.004	-4.16 ± 0.05
	4	0.1883	0.208 ± 0.007	-1.93 ± 0.08		4	0.1939	0.209 ± 0.008	-1.92 ± 0.08
		0.6238	0.306 ± 0.006	-2.92 ± 0.08			0.6818	0.306 ± 0.005	-2.87 ± 0.07
		2.1388	0.403 ± 0.004	-4.11 ± 0.06			2.4372	0.400 ± 0.005	-4.06 ± 0.05
	5	0.2869	0.208 ± 0.007	-1.85 ± 0.07		5	0.3035	0.208 ± 0.005	-1.83 ± 0.06
		0.9243	0.306 ± 0.005	-2.85 ± 0.07			1.0256	0.307 ± 0.005	-2.81 ± 0.07
		2.9593	0.403 ± 0.004	-4.06 ± 0.06			3.3920	0.401 ± 0.003	-4.01 ± 0.05
15	2	0.0653	0.219 ± 0.009	-1.64 ± 0.07	18	2	0.0523	0.220 ± 0.009	-1.83 ± 0.07
		0.2171	0.311 ± 0.006	-2.24 ± 0.06			0.1973	0.312 ± 0.007	-2.41 ± 0.06
		0.8519	0.404 ± 0.004	-2.98 ± 0.05			0.8940	0.403 ± 0.004	-3.17 ± 0.05
	3	0.1639	0.212 ± 0.007	-1.40 ± 0.06		3	0.1620	0.211 ± 0.006	-1.51 ± 0.05
		0.5151	0.307 ± 0.006	-2.06 ± 0.05			0.5372	0.309 ± 0.005	-2.20 ± 0.05
		1.6703	0.404 ± 0.004	-2.87 ± 0.04			1.8454	0.403 ± 0.003	-3.04 ± 0.03
	4	0.2626	0.209 ± 0.006	-1.30 ± 0.05		4	0.2717	0.211 ± 0.007	-1.41 ± 0.05
		0.8158	0.306 ± 0.005	-1.99 ± 0.05			0.8809	0.307 ± 0.005	-2.10 ± 0.05
		2.4916	0.404 ± 0.004	-2.83 ± 0.05			2.8006	0.402 ± 0.004	-2.98 ± 0.04
	5	0.3613	0.208 ± 0.006	-1.26 ± 0.05		5	0.3815	0.209 ± 0.005	-1.34 ± 0.05
		1.1176	0.306 ± 0.005	-1.95 ± 0.05			1.2260	0.306 ± 0.005	-2.05 ± 0.05
		3.3140	0.403 ± 0.004	-2.79 ± 0.05			3.7575	0.403 ± 0.003	-2.96 ± 0.04

Table 5. *NPT* MC simulation results along the coexistence curve for selected symmetric diblock 4-mer and 8-mer fluids. See table 2 for details.

System	T^*	η	E^*	System	T^*	η	E^*
3	1.2	0.452 ± 0.004	-7.31 ± 0.07	10	1.8	0.401 ± 0.003	-5.86 ± 0.07
	1.3	0.442 ± 0.005	-7.10 ± 0.08		1.9	0.395 ± 0.004	-5.82 ± 0.08
	1.4	0.433 ± 0.005	-6.90 ± 0.08		2.0	0.388 ± 0.004	-5.70 ± 0.07
	1.5	0.423 ± 0.006	-6.72 ± 0.10		2.1	0.380 ± 0.006	-5.54 ± 0.09
	1.6	0.413 ± 0.005	-6.50 ± 0.10		2.2	0.373 ± 0.005	-5.40 ± 0.09
	1.7	0.403 ± 0.006	-6.30 ± 0.11		2.3	0.358 ± 0.006	-5.13 ± 0.10
4	0.9	0.451 ± 0.004	-5.46 ± 0.05	11	1.3	0.403 ± 0.004	-4.48 ± 0.07
	1.0	0.438 ± 0.005	-5.23 ± 0.06		1.4	0.393 ± 0.003	-4.35 ± 0.07
	1.1	0.424 ± 0.005	-5.03 ± 0.07		1.5	0.389 ± 0.004	-4.28 ± 0.07
	1.2	0.410 ± 0.006	-4.81 ± 0.08		1.6	0.374 ± 0.005	-4.11 ± 0.06
	1.3	0.397 ± 0.007	-4.62 ± 0.09		1.7	0.358 ± 0.006	-3.91 ± 0.07
5	0.76	0.402 ± 0.008	-3.13 ± 0.06	12	0.86	0.392 ± 0.003	-2.89 ± 0.03
	0.80	0.394 ± 0.007	-3.04 ± 0.06		0.90	0.382 ± 0.004	-2.85 ± 0.05
					0.95	0.370 ± 0.005	-2.79 ± 0.04
					1.00	0.356 ± 0.009	-2.73 ± 0.06
					1.05	0.344 ± 0.010	-2.66 ± 0.05

Table 6. GEMC simulation results for selected symmetric diblock 4-mer and 8-mer fluids. The fixed variables during the simulation are defined as for table 2. The densities η, number of molecules N and reduced energies per segment E^* in the coexisting vapor and liquid phases are labeled v and l, respectively.

System	T^*	η_l	η_v	N_l	N_v	E_l^*	E_v^*
3	1.7	0.403 ± 0.006	0.0005 ± 0.0000	138	118	-6.28 ± 0.11	-0.49 ± 0.03
	1.8	0.391 ± 0.004	0.0011 ± 0.0004	240	16	-6.05 ± 0.08	-0.54 ± 0.11
	1.9	0.382 ± 0.005	0.0023 ± 0.0010	228	28	-5.86 ± 0.10	-0.60 ± 0.11
	2.0	0.371 ± 0.007	0.0034 ± 0.0003	193	63	-5.64 ± 0.11	-0.62 ± 0.07
	2.1	0.356 ± 0.008	0.0054 ± 0.0008	182	74	-5.36 ± 0.14	-0.66 ± 0.07
	2.2	0.343 ± 0.009	0.0097 ± 0.0007	177	79	-5.14 ± 0.14	-0.78 ± 0.09
	2.3	0.324 ± 0.013	0.0159 ± 0.0016	69	187	-4.82 ± 0.20	-0.92 ± 0.11
	2.4	0.304 ± 0.012	0.0292 ± 0.0082	224	32	-4.49 ± 0.16	-1.16 ± 0.28
4	1.3	0.396 ± 0.004	0.0006 ± 0.0002	251	5	-4.60 ± 0.05	-0.44 ± 0.14
	1.4	0.379 ± 0.006	0.0015 ± 0.0004	245	11	-4.37 ± 0.07	-0.46 ± 0.10
	1.5	0.362 ± 0.006	0.0034 ± 0.0005	228	28	-4.13 ± 0.08	-0.50 ± 0.08
	1.6	0.343 ± 0.009	0.0080 ± 0.0011	166	90	-3.87 ± 0.10	-0.60 ± 0.08
	1.7	0.319 ± 0.012	0.0159 ± 0.0028	190	66	-3.58 ± 0.12	-0.74 ± 0.10
	1.8	0.277 ± 0.018	0.0284 ± 0.0076	223	33	-3.17 ± 0.14	-0.89 ± 0.20
5	0.80	0.394 ± 0.005	0.0007 ± 0.0003	251	5	-3.04 ± 0.04	-0.37 ± 0.12
	0.85	0.381 ± 0.006	0.0023 ± 0.0007	243	13	-2.94 ± 0.05	-0.46 ± 0.17
	0.90	0.366 ± 0.006	0.0024 ± 0.0006	238	18	-2.79 ± 0.04	-0.40 ± 0.09
	0.95	0.352 ± 0.008	0.0051 ± 0.0008	202	54	-2.66 ± 0.06	-0.45 ± 0.08
	1.00	0.330 ± 0.010	0.0101 ± 0.0009	165	91	-2.49 ± 0.07	-0.56 ± 0.08
	1.05	0.307 ± 0.015	0.0201 ± 0.0049	184	72	-2.33 ± 0.08	-0.71 ± 0.14
	1.10	0.268 ± 0.019	0.0285 ± 0.0092	229	27	-2.11 ± 0.09	-0.72 ± 0.20
10	2.3	0.361 ± 0.006	0.0069 ± 0.0002	141	115	-5.18 ± 0.09	-2.48 ± 0.34
	2.4	0.352 ± 0.007	0.0030 ± 0.0001	98	158	-5.00 ± 0.11	-1.07 ± 0.05
	2.5	0.327 ± 0.011	0.0031 ± 0.0002	93	163	-4.62 ± 0.15	-1.02 ± 0.08
	2.68	0.294 ± 0.019	0.0101 ± 0.0008	64	192	-4.15 ± 0.22	-1.14 ± 0.07
11	1.70	0.358 ± 0.005	0.0025 ± 0.0001	142	114	-3.90 ± 0.06	-0.86 ± 0.04
	1.78	0.343 ± 0.008	0.0026 ± 0.0001	133	123	-3.72 ± 0.09	-0.82 ± 0.12
	1.85	0.335 ± 0.008	0.0061 ± 0.0002	146	110	-3.61 ± 0.09	-0.93 ± 0.06
	1.90	0.315 ± 0.010	0.0069 ± 0.0004	142	114	-3.38 ± 0.10	-0.91 ± 0.09
	1.95	0.299 ± 0.014	0.0077 ± 0.0004	116	140	-3.24 ± 0.12	-0.92 ± 0.06
	2.05	0.238 ± 0.074	0.0190 ± 0.0039	101	155	-2.71 ± 0.55	-1.07 ± 0.09
12	0.95	0.374 ± 0.005	0.0026 ± 0.0000	130	126	-2.85 ± 0.04	-2.19 ± 0.08
	1.00	0.358 ± 0.007	0.0027 ± 0.0001	123	133	-2.79 ± 0.05	-2.14 ± 0.07
	1.05	0.341 ± 0.008	0.0070 ± 0.0002	136	120	-2.62 ± 0.04	-2.09 ± 0.06
	1.10	0.337 ± 0.008	0.0057 ± 0.0004	172	84	-2.57 ± 0.05	-1.39 ± 0.12
	1.15	0.315 ± 0.011	0.0067 ± 0.0004	147	109	-2.42 ± 0.08	-1.07 ± 0.08
	1.20	0.288 ± 0.015	0.0084 ± 0.0004	97	159	-2.26 ± 0.09	-0.84 ± 0.06
	1.25	0.269 ± 0.015	0.0378 ± 0.0041	156	100	-2.15 ± 0.07	-1.34 ± 0.09

In order to obtain a comprehensive understanding of the thermodynamic properties of the systems studied and fully test the hetero-SAFT-VR approach, we have also determined phase diagrams for the symmetric 4-mer (systems 3–5, as shown in figure 8) and 8-mer (systems 10–12, as shown in figure 9) fluids with a segment diameter ratio of $\sigma_2/\sigma_1 = 2$, a potential range of $\lambda_1 = \lambda_2 = 1.5$ and differing potential depth ratios of $\varepsilon_2/\varepsilon_1 = 0.5$, 1.0, and 1.5. If we compare the phase diagrams for all of the symmetric 4-mer and 8-mer fluids studied, we can see that the critical temperature of the diblock chain fluids increases with an increase in the ratio of $\varepsilon_2/\varepsilon_1$; which is to be anticipated as the attractive interactions between the molecules have increased. Additionally, as expected from the phase behaviour of homonuclear fluids, as the chain length increases the critical point moves to higher temperatures and the phase envelope narrows. In all cases, excellent agreement is achieved between the hetero-SAFT-VR predictions and the simulation data for both the gas and liquid coexisting densities, though we note the theory over-predicts the critical point. This shortcoming of the SAFT-VR approach has been addressed for homonuclear chains in recent work by the

Table 7. GEMC simulation results for asymmetric diblock 6-mer and 8-mer fluids. See table 6 for details.

System	T^*	η_l	η_v	N_l	N_v	E_l^*	E_v^*
13	2.10	0.363 ± 0.006	0.0021 ± 0.0001	131	125	-5.00 ± 0.10	-0.84 ± 0.08
	2.20	0.351 ± 0.009	0.0039 ± 0.0001	131	125	-4.82 ± 0.13	-0.80 ± 0.11
	2.30	0.335 ± 0.012	0.0070 ± 0.0006	92	164	-4.55 ± 0.17	-0.93 ± 0.07
	2.40	0.315 ± 0.011	0.0106 ± 0.0007	141	115	-4.26 ± 0.13	-1.00 ± 0.07
	2.45	0.307 ± 0.016	0.0151 ± 0.0016	83	173	-4.14 ± 0.19	-1.08 ± 0.07
14	1.50	0.386 ± 0.007	0.0007 ± 0.0000	135	121	-4.31 ± 0.09	-0.72 ± 0.13
	1.60	0.371 ± 0.006	0.0020 ± 0.0000	138	118	-4.12 ± 0.08	-0.76 ± 0.08
	1.65	0.364 ± 0.006	0.0036 ± 0.0001	144	112	-4.02 ± 0.08	-0.64 ± 0.10
	1.70	0.354 ± 0.007	0.0039 ± 0.0001	128	128	-3.88 ± 0.08	-0.69 ± 0.12
	1.80	0.333 ± 0.009	0.0095 ± 0.0010	181	75	-3.63 ± 0.10	-0.91 ± 0.07
	1.85	0.317 ± 0.012	0.0105 ± 0.0007	133	123	-3.46 ± 0.12	-0.90 ± 0.06
	1.90	0.297 ± 0.017	0.0133 ± 0.0013	68	168	-3.27 ± 0.15	-0.92 ± 0.06
15	1.00	0.384 ± 0.007	0.0007 ± 0.0000	151	105	-3.25 ± 0.07	-0.79 ± 0.12
	1.05	0.371 ± 0.007	0.0018 ± 0.0001	151	105	-3.14 ± 0.06	-1.12 ± 0.13
	1.10	0.350 ± 0.010	0.0037 ± 0.0002	148	108	-3.00 ± 0.08	-1.57 ± 0.24
	1.15	0.342 ± 0.010	0.0072 ± 0.0007	157	99	-2.91 ± 0.08	-1.38 ± 0.16
	1.17	0.331 ± 0.010	0.0082 ± 0.0007	156	100	-2.82 ± 0.08	-1.38 ± 0.14
	1.20	0.328 ± 0.009	0.0082 ± 0.0009	177	79	-2.79 ± 0.07	-0.95 ± 0.10
	1.23	0.308 ± 0.013	0.0084 ± 0.0015	177	79	-2.67 ± 0.07	-0.87 ± 0.09
	1.25	0.300 ± 0.017	0.0119 ± 0.0008	129	127	-2.62 ± 0.08	-1.03 ± 0.11
16	2.10	0.360 ± 0.007	0.0007 ± 0.0000	109	147	-4.71 ± 0.11	-0.91 ± 0.13
	2.20	0.354 ± 0.007	0.0021 ± 0.0001	136	120	-4.57 ± 0.11	-0.94 ± 0.09
	2.30	0.338 ± 0.009	0.0033 ± 0.0001	124	132	-4.36 ± 0.12	-0.97 ± 0.06
	2.40	0.312 ± 0.014	0.0053 ± 0.0003	104	152	-4.00 ± 0.16	-0.99 ± 0.07
	2.50	0.303 ± 0.013	0.0131 ± 0.0007	110	146	-3.87 ± 0.16	-1.15 ± 0.06
17	1.55	0.386 ± 0.005	0.0002 ± 0.0000	132	124	-4.24 ± 0.07	-0.81 ± 0.19
	1.60	0.376 ± 0.005	0.0004 ± 0.0000	138	118	-4.12 ± 0.06	-0.88 ± 0.14
	1.65	0.369 ± 0.007	0.0006 ± 0.0000	106	150	-4.01 ± 0.08	-0.83 ± 0.15
	1.70	0.363 ± 0.007	0.0011 ± 0.0000	113	143	-3.96 ± 0.08	-0.86 ± 0.14
	1.75	0.355 ± 0.008	0.0022 ± 0.0001	109	147	-3.83 ± 0.08	-0.93 ± 0.08
	1.80	0.340 ± 0.008	0.0020 ± 0.0001	137	119	-3.67 ± 0.08	-0.90 ± 0.07
	1.85	0.333 ± 0.011	0.0038 ± 0.0002	89	167	-3.58 ± 0.12	-0.94 ± 0.06
	1.90	0.319 ± 0.005	0.0108 ± 0.0003	110	146	-3.44 ± 0.09	-0.92 ± 0.08
18	1.20	0.361 ± 0.007	0.0010 ± 0.0000	126	130	-3.22 ± 0.08	-0.91 ± 0.08
	1.25	0.348 ± 0.008	0.0014 ± 0.0001	148	108	-3.12 ± 0.07	-0.96 ± 0.08
	1.30	0.331 ± 0.009	0.0031 ± 0.0001	151	105	-3.01 ± 0.06	-1.01 ± 0.07
	1.35	0.313 ± 0.011	0.0050 ± 0.0006	162	94	-2.87 ± 0.07	-1.06 ± 0.13
	1.40	0.303 ± 0.011	0.0109 ± 0.0005	135	121	-2.74 ± 0.06	-1.16 ± 0.08

authors [24, 29, 30, 72], and will be extended to heteronuclear chains in future work.

Finally, in order to get a better understanding of the effect of molecular structure on the coexistence properties we have considered the phase equilibrium of asymmetric 6-mer (systems 13–15, as shown in figure 10) and asymmetric 8-mer fluids (systems 16–18, as shown in figure 11) with three different potential depth ratios. In contrast to the symmetric diblock 8-mer fluid with $\varepsilon_2/\varepsilon_1 = 1.5$ (system 10), the asymmetric 8-mer with $\varepsilon_2/\varepsilon_1 = 1.5$ (system 16) has a lower critical temperature; however, the asymmetric diblock 8-mer fluid with $\varepsilon_2/\varepsilon_1 = 0.5$ (system 18) has a higher critical temperature than the corresponding symmetric 8-mer fluid (system 12). It is also observed that the coexistence curve for the asymmetric 8-mer fluid with $\varepsilon_2 = \varepsilon_1$ (system 17) crosses that of the asymmetric 8-mer fluid with $\varepsilon_2 = \varepsilon_1$ (system 11). For the systems with the same value of $\varepsilon_2/\varepsilon_1$, the asymmetric 6-mer fluids have a higher critical point than the symmetric 4-mer fluids and a lower critical point than the asymmetric 8-mer fluids due to chain length effects. From the figures we see that

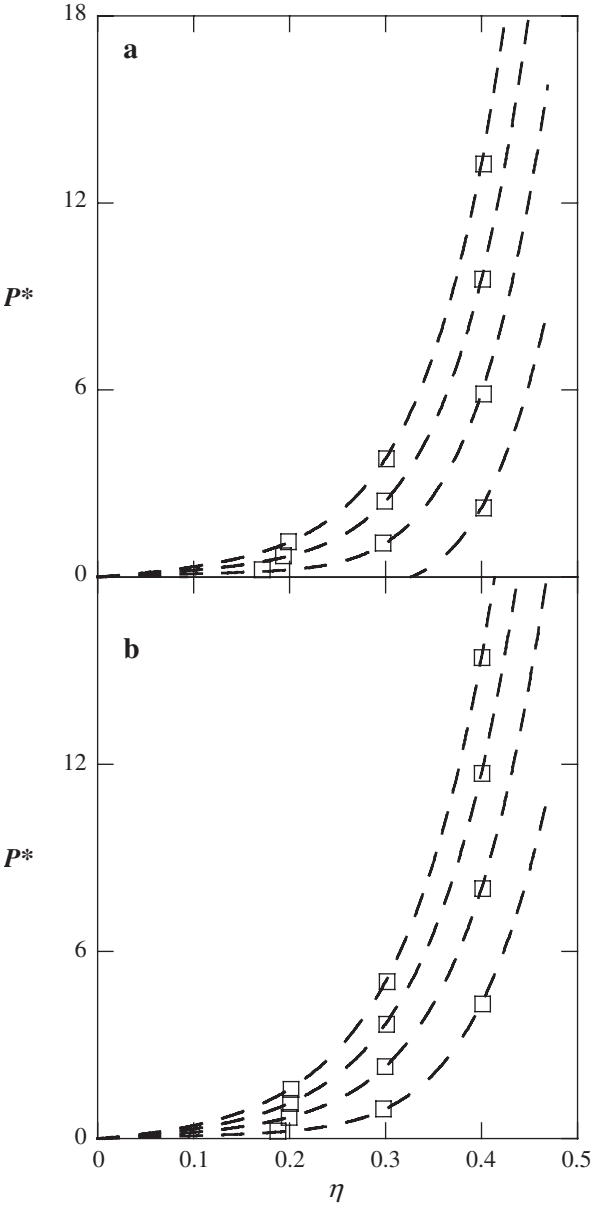

Figure 1. Isotherms for symmetric diblock 4-mer fluids with (*a*) diameter $\sigma_2=\sigma_1$, well depth $\varepsilon_2=1.5\varepsilon_1$ and range $\lambda_1=\lambda_2=1.5$ (system 1) and (*b*) diameter $\sigma_2=\sigma_1$, well depth $\varepsilon_2=0.5\varepsilon_1$ and range $\lambda_1=\lambda_2=1.5$ (system 2). SAFT-VR EOS results at T^*=2.0, 3.0, 4.0, 5.0 (from bottom to top) are represented as continuous curves and the squares represent the *NPT* MC simulation data.

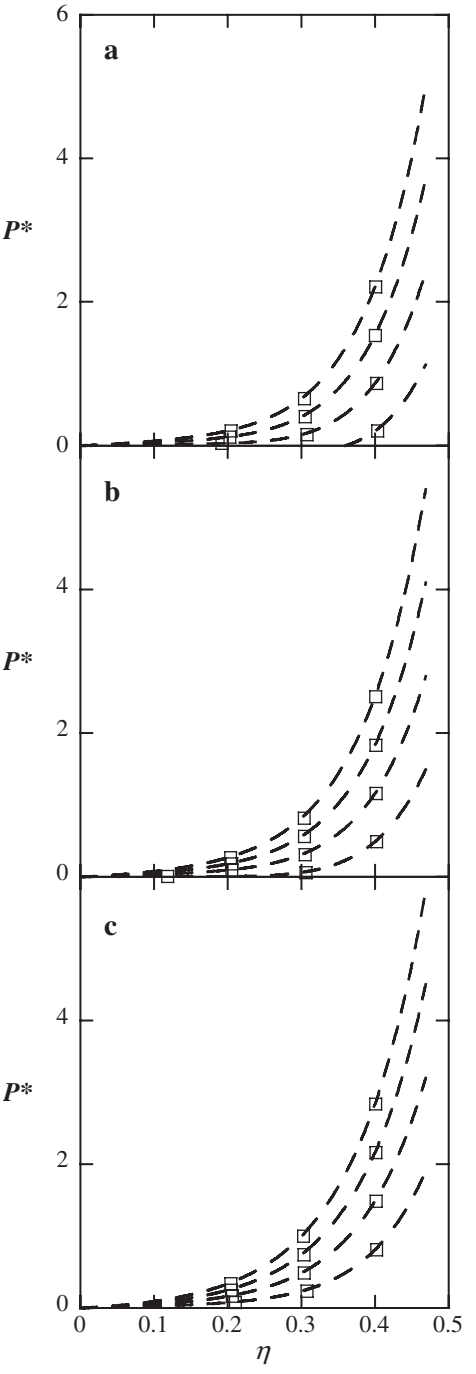

Figure 2. Isotherms for symmetric diblock 4-mer fluids with (*a*) diameter $\sigma_2=2\sigma_1$, well depth $\varepsilon_2=1.5\varepsilon_1$ and range $\lambda_1=\lambda_2=1.5$ (system 3), (*b*) diameter $\sigma_2=2\sigma_1$, well depth $\varepsilon_2=\varepsilon_1$ and range $\lambda_1=\lambda_2=1.5$ (system 4) and (*c*) diameter $\sigma_2=2\sigma_1$, well depth $\varepsilon_2=0.5\varepsilon_1$ and range $\lambda_1=\lambda_2=1.5$ (system 5). SAFT-VR EOS results at T^*=2.0, 3.0, 4.0, 5.0 (from bottom to top) are represented as continuous curves and the symbols represent the *NPT* MC simulation data.

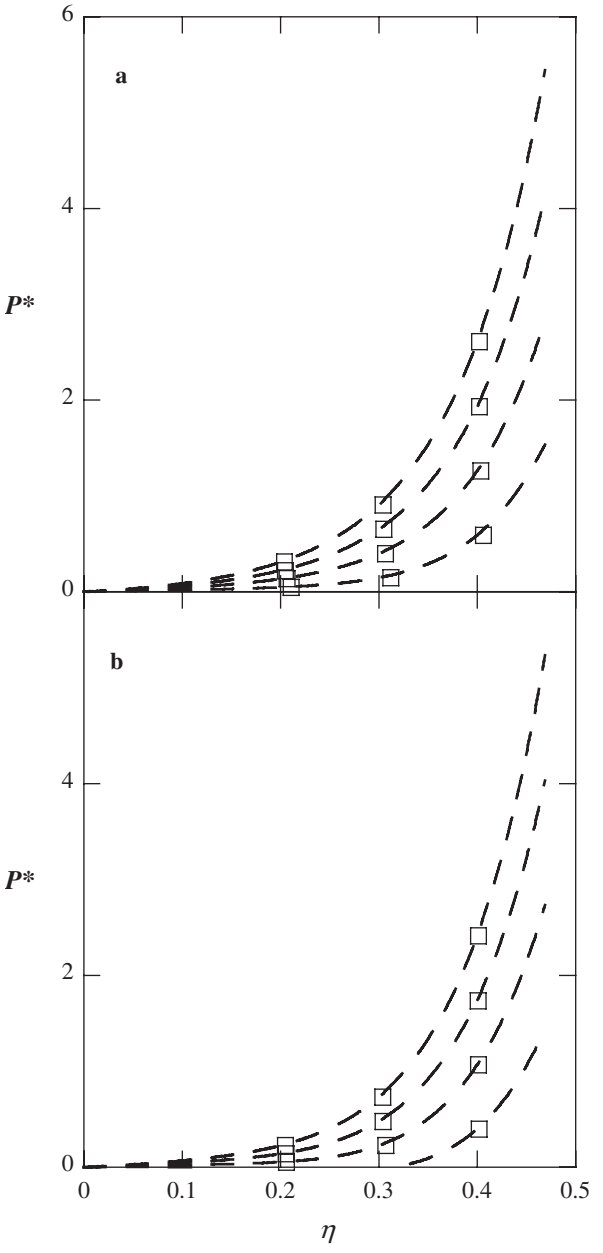

Figure 3. Isotherms for symmetric diblock 4-mer fluids with (*a*) diameter $\sigma_2 = 2\sigma_1$, well depth $\varepsilon_2 = \varepsilon_1$ and range $\lambda_1 = \lambda_2 = 1.4$ (system 6) and (*b*) diameter $\sigma_2 = 2\sigma_1$, well depth $\varepsilon_2 = \varepsilon_1$ and range $\lambda_1 = \lambda_2 = 1.6$ (system 7). SAFT-VR EOS results at $T^* = 2.0, 3.0, 4.0, 5.0$ (from bottom to top) are represented as continuous curves and the symbols represent the *NPT* MC simulation data.

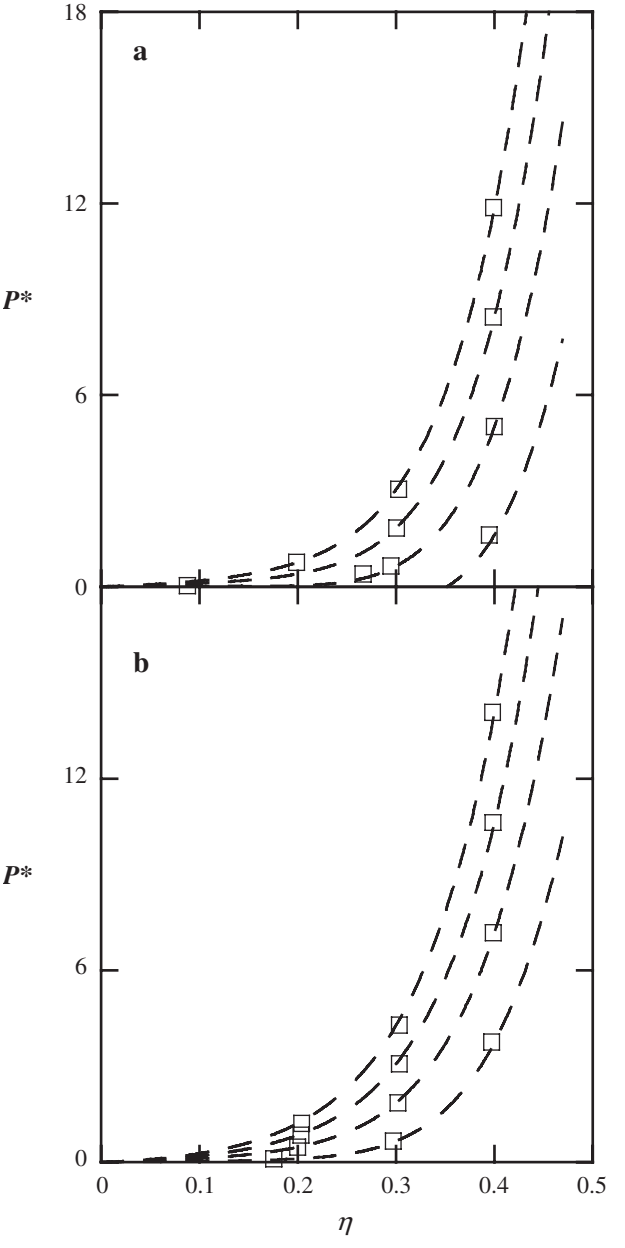

Figure 4. Isotherms for symmetric diblock 8-mer fluids with (*a*) diameter $\sigma_2 = \sigma_1$, well depth $\varepsilon_2 = 1.5\varepsilon_1$ and range $\lambda_1 = \lambda_2 = 1.5$ (system 8) and (*b*) diameter $\sigma_2 = \sigma_1$, well depth $\varepsilon_2 = 0.5\varepsilon_1$ and range $\lambda_1 = \lambda_2 = 1.5$ (system 9). SAFT-VR EOS results at $T^* = 2.0, 3.0, 4.0, 5.0$ (from bottom to top) are represented as continuous curves and the symbols represent the *NPT* MC simulation data.

the hetero-SAFT-VR prediction agrees well with the simulation results for the asymmetric fluids, indicating that the theory is able to capture the effect of having chains of different molecular structure, but equal chain length, on the phase behaviour.

5. Conclusion

In this work, the SAFT-VR approach has been extended to study hetero-segmented chain fluids, with particular focus on symmetric and asymmetric diblock chains.

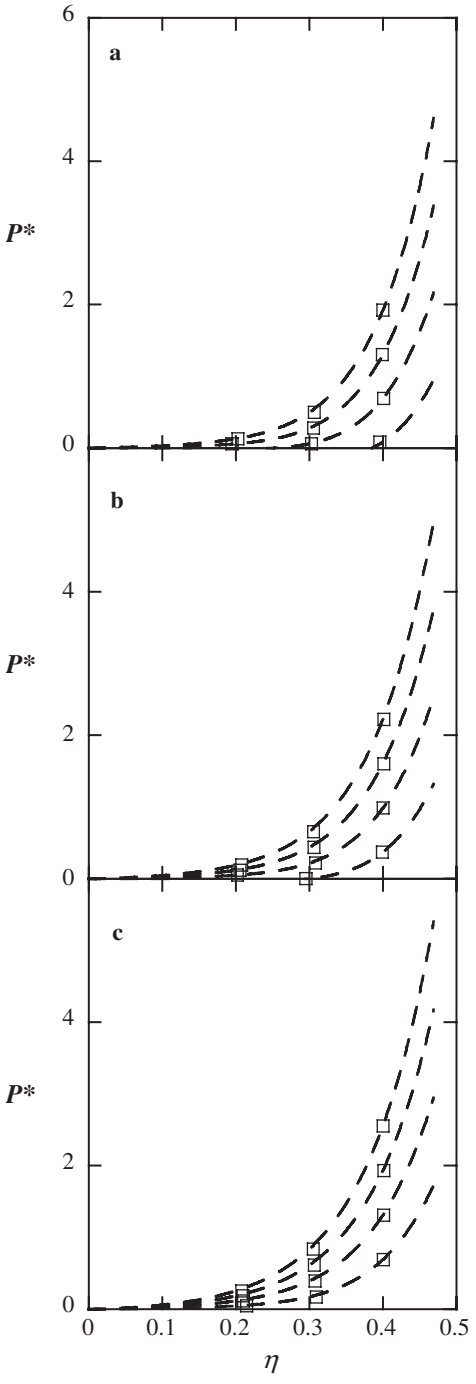

Figure 5. Isotherms for symmetric diblock 8-mer fluids with (*a*) diameter $\sigma_2 = 2\sigma_1$, well depth $\varepsilon_2 = 1.5\varepsilon_1$ and range $\lambda_1 = \lambda_2 = 1.5$ (system 10), (*b*) diameter $\sigma_2 = 2\sigma_1$, well depth $\varepsilon_2 = \varepsilon_1$ and range $\lambda_1 = \lambda_2 = 1.5$ (system 11) and (*c*) diameter $\sigma_2 = 2\sigma_1$, well depth $\varepsilon_2 = 0.5\varepsilon_1$ and range $\lambda_1 = \lambda_2 = 1.5$ (system 12). SAFT-VR EOS results at $T^* = 2.0, 3.0, 4.0, 5.0$ (from bottom to top) are represented as continuous curves and the symbols represent the *NPT* MC simulation data.

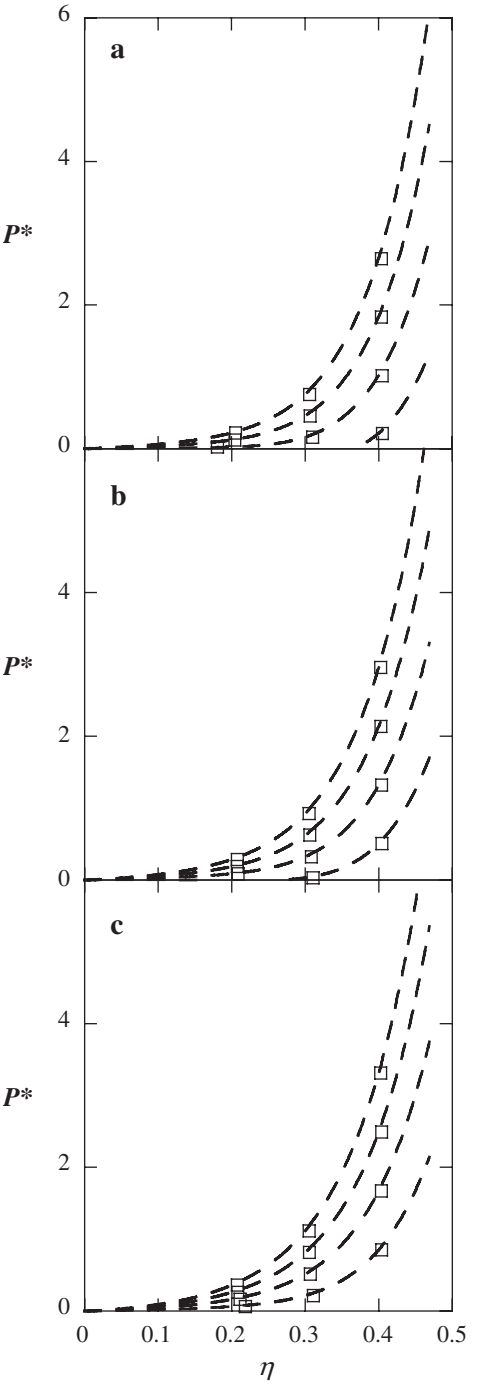

Figure 6. Isotherms for asymmetric diblock 6-mer fluids with $m_1 = 4$, $m_2 = 2$ and (*a*) diameter $\sigma_2 = 2\sigma_1$, well depth $\varepsilon_2 = 1.5\varepsilon_1$ and range $\lambda_1 = \lambda_2 = 1.5$ (system 13), (*b*) diameter $\sigma_2 = 2\sigma_1$, well depth $\varepsilon_2 = \varepsilon_1$ and range $\lambda_1 = \lambda_2 = 1.5$ (system 14) and (*c*) diameter $\sigma_2 = 2\sigma_1$, well depth $\varepsilon_2 = 0.5\varepsilon_1$ and range $\lambda_1 = \lambda_2 = 1.5$ (system 15). SAFT-VR EOS results at $T^* = 2.0, 3.0, 4.0, 5.0$ (from bottom to top) are represented as continuous curves and the squares represent the *NPT* MC simulation data.

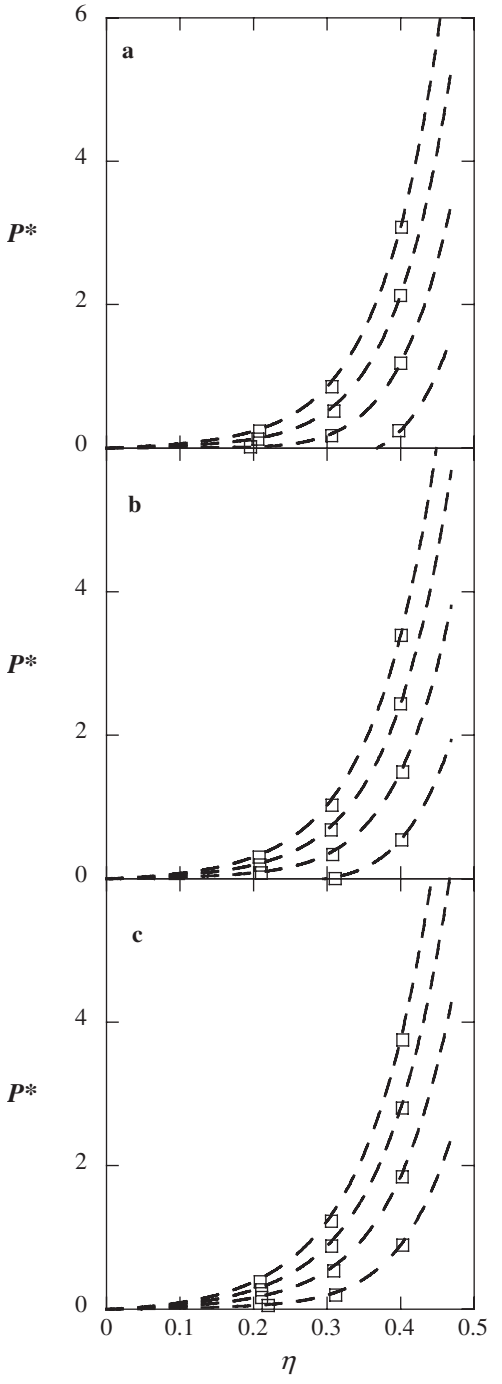

Figure 7. Isotherms for asymmetric diblock 8-mer fluids with $m_1=6$, $m_2=2$ and (*a*) diameter $\sigma_2=2\sigma_1$, well depth $\varepsilon_2=1.5\varepsilon_1$ and range $\lambda_1=\lambda_2=1.5$ (system 16), (*b*) diameter $\sigma_2=2\sigma_1$, well depth $\varepsilon_2=\varepsilon_1$ and range $\lambda_1=\lambda_2=1.5$ (system 17) and (*c*) diameter $\sigma_2=2\sigma_1$, well depth $\varepsilon_2=0.5\varepsilon_1$ and range $\lambda_1=\lambda_2=1.5$ (system 18). SAFT-VR EOS results at $T^*=2.0, 3.0, 4.0, 5.0$ (from bottom to top) are represented as continuous curves and the squares represent the *NPT* MC simulation data.

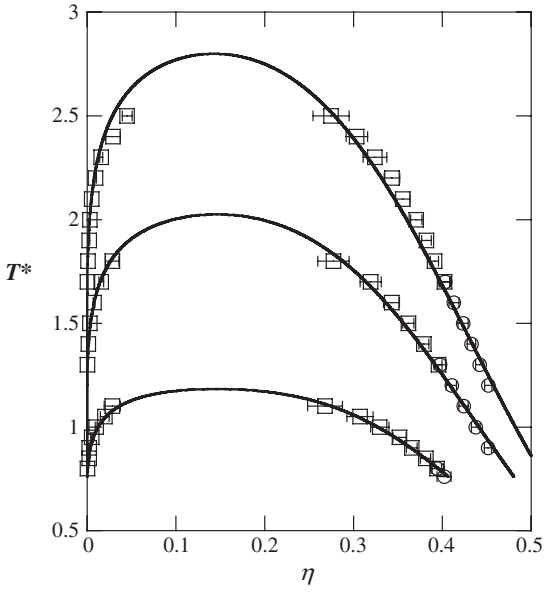

Figure 8. Phase equilibrium for symmetric diblock 4-mer fluids with (from top to bottom) diameter $\sigma_2=2\sigma_1$, well depth $\varepsilon_2=1.5\varepsilon_1$ and range $\lambda_1=\lambda_2=1.5$ (system 3), diameter $\sigma_2=2\sigma_1$, well depth $\varepsilon_2=\varepsilon_1$ and range $\lambda_1=\lambda_2=1.5$ (system 4), and diameter $\sigma_2=2\sigma_1$, well depth $\varepsilon_2=0.5\varepsilon_1$ and range $\lambda_1=\lambda_2=1.5$ (system 5). Hetero-SAFT-VR results are represented as continuous curves, the squares and circles correspond to GEMC and *NPT* MC simulation data, respectively.

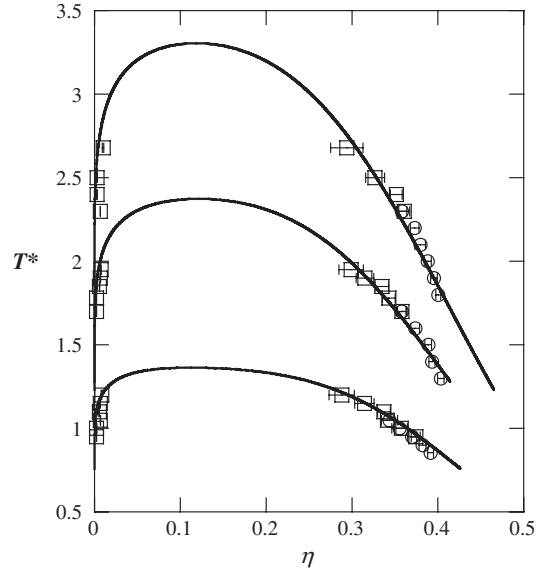

Figure 9. Phase equilibrium for symmetric diblock 8-mer fluids with (from top to bottom) diameter $\sigma_2=2\sigma_1$, well depth $\varepsilon_2=1.5\varepsilon_1$ and range $\lambda_1=\lambda_2=1.5$ (system 10); diameter $\sigma_2=2\sigma_1$, well depth $\varepsilon_2=\varepsilon_1$ and range $\lambda_1=\lambda_2=1.5$ (system 11); and diameter $\sigma_2=2\sigma_1$, well depth $\varepsilon_2=0.5\varepsilon_1$ and range $\lambda_1=\lambda_2=1.5$ (system 12). Hetero-SAFT-VR results are represented as continuous curves, and the squares and circles correspond to GEMC and *NPT* MC simulation data, respectively.

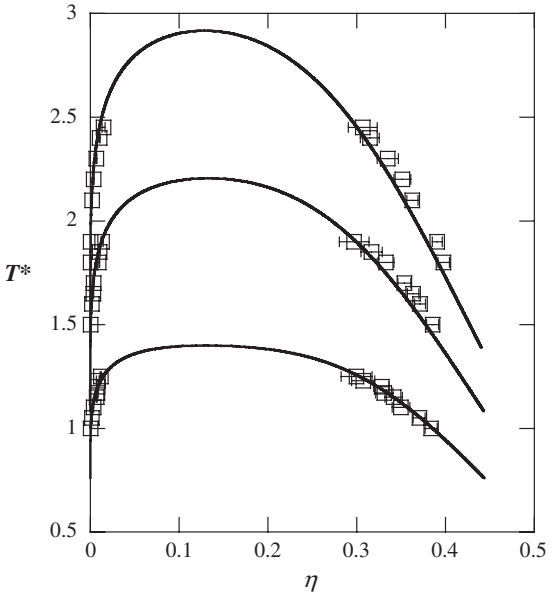

Figure 10. Phase equilibrium for asymmetric diblock 6-mer fluids with (from top to bottom) $m_1 = 4$, $m_2 = 2$ and diameter $\sigma_2 = 2\sigma_1$, well depth $\varepsilon_2 = 1.5\varepsilon_1$ and range $\lambda_1 = \lambda_2 = 1.5$ (system 13), diameter $\sigma_2 = 2\sigma_1$, well depth $\varepsilon_2 = \varepsilon_1$ and range $\lambda_1 = \lambda_2 = 1.5$ (system 14), and diameter $\sigma_2 = 2\sigma_1$, well depth $\varepsilon_2 = 0.5\varepsilon_1$ and range $\lambda_1 = \lambda_2 = 1.5$ (system 15). Hetero-SAFT-VR results are represented as continuous curves, and the squares correspond to GEMC simulation data.

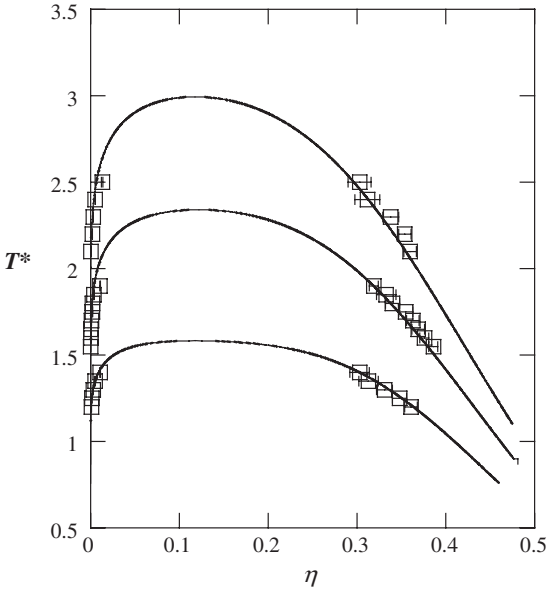

Figure 11. Phase equilibrium for asymmetric diblock 8-mer fluids with (from top to bottom) $m_1 = 6$, $m_2 = 2$ and diameter $\sigma_2 = 2\sigma_1$, well depth $\varepsilon_2 = 1.5\varepsilon_1$ and range $\lambda_1 = \lambda_2 = 1.5$ (system 16), diameter $\sigma_2 = 2\sigma_1$, well depth $\varepsilon_2 = \varepsilon_1$ and range $\lambda_1 = \lambda_2 = 1.5$ (system 17), and diameter $\sigma_2 = 2\sigma_1$, well depth $\varepsilon_2 = 0.5\varepsilon_1$ and range $\lambda_1 = \lambda_2 = 1.5$ (system 18). Hetero-SAFT-VR results are represented as continuous curves, and the squares correspond to the GEMC simulation data.

Eighteen systems differing in chain length, segment size, potential range, potential well depth, and molecular structure have been examined. In order to gain a comprehensive understanding of the thermodynamic properties of the systems studied and test the hetero-SAFT-VR approach, both *NPT* MC and GEMC simulation methods were utilized to validate the theoretical predictions. The phase behaviour of the diblock fluids is found to be affected by the interaction energies, segment size and the distribution of segments in terms of symmetry, i.e. at a given pressure and temperature, the fluid density rises as the ratio of interaction energy and/or segment size increases, as the potential range increases, as the chain length increases, and as the fraction of smaller segments decreases. The critical temperature of the diblock chain fluids rises as the ratio of $\varepsilon_2/\varepsilon_1$ increases, and as the chain length increases. Excellent agreement between the theoretical predictions and simulation results has been achieved. The average absolute deviation (AAD) between the hetero-SAFT-VR predictions and the simulation data for all systems is 1–3%. Slightly larger deviations (4–10%) are seen at low pressures and for the lowest temperature ($T^* = 2$) studied. In future work, we will apply the hetero-SAFT-VR approach to study more realistic systems such as polymers and small molecules composed of different functional groups.

Acknowledgements

The authors gratefully acknowledge the National Science Foundation for supporting this work under grant numbers CTS-0452688 and DMR-0103399. We also thank Pedro Morgado, Felipe Blas and Eduardo Felipe for useful discussions.

References

[1] E. A. Muller and K. E. Gubbins, in *Equations of State for Fluids and Fluid Mixtures*, edited by J. V. Sengers, R. F. Kayser, C. J. Peters, and H. J. White, Part II (Elsevier, Amsterdam, 2000), p. 435.
[2] S. M. Lambert, Y. H. Song, and J. M. Prausnitz, in *Equations of State for Fluids and Fluid Mixtures*, edited by J. V. Sengers, R. F. Kayser, C. J. Peters, and H. J. White, Part II (Elsevier, Amsterdam, 2000), p. 523.
[3] I. G. Economou, Ind. Engng Chem. Res. **41,** 953 (2002).
[4] E. A. Muller and K. E. Gubbins, Ind. Engng Chem. Res. **40,** 2193 (2001).
[5] H. Adidharma and M. Radosz, Ind. Engng Chem. Res. **37,** 4453 (1998).
[6] C. K. Chen, M. Banaszak, and M. Radosz, J. Phys. Chem. B **102,** 2427 (1998).

[7] F. J. Blas and L. F. Vega, Ind. Engng Chem. Res. **37,** 660 (1998).
[8] G. Sadowski, Fluid Phase Equilibria **149,** 75 (1998).
[9] C. McCabe and G. Jackson, Phys. Chem. Chem. Phys. **1,** 2057 (1999).
[10] J. Jiang and J. M. Prausnitz, J. Chem. Phys. **111,** 5964 (1999).
[11] M. L. L. Paredes, R. Nobrega, and F. W. Tavares, Ind. Engng Chem. Res. **40,** 1748 (2001).
[12] J. C. Pamies and L. F. Vega, Molec. Phys. **100,** 2519 (2002).
[13] T. Kraska and K. E. Gubbins, Ind. Engng Chem. Res. **35,** 4727 (1996).
[14] M. S. Wertheim, J. Statist. Phys. **35,** 19 (1984).
[15] M. S. Wertheim, J. Statist. Phys. **35,** 35 (1984).
[16] M. S. Wertheim, J. Statist. Phys. **42,** 459 (1986).
[17] M. S. Wertheim, J. Statist. Phys. **42,** 477 (1986).
[18] A. Gil Villegas, A. Galindo, P. J. Whitehead, S. J. Mills, G. Jackson, and A. N. Burgess, J. Chem. Phys. **106,** 4168 (1997).
[19] A. Galindo, L. A. Davies, A. Gil-Villegas, and G. Jackson, Molec. Phys. **93,** 241 (1998).
[20] C. McCabe, A. Galindo, A. Gil-Villegas, and G. Jackson, Int. J. Thermophys. **19,** 1511 (1998).
[21] C. McCabe, A. Gil-Villegas, and G. Jackson, J. Phys. Chem. B **102,** 4183 (1998).
[22] C. McCabe, A. Galindo, M. N. Garcia-Lisbona, and G. Jackson, Ind. Engng Chem. Res. **40,** 3835 (2001).
[23] C. McCabe, S. Kiselev. Ind. Engng Chem. Res., in press.
[24] C. McCabe and S. B. Kiselev, Fluid Phase Equilibria **219,** 3 (2004).
[25] A. Galindo, L. J. Florusse, and C. J. Peters, Fluid Phase Equilibria **160,** 123 (1999).
[26] E. J. M. Filipe, E. de Azevedo, L. F. G. Martins, V. A. M. Soares, J. C. G. Calado, C. McCabe, and G. Jackson, J. Phys. Chem. B **104,** 1315 (2000).
[27] E. J. M. Filipe, L. F. G. Martins, J. C. G. Calado, C. McCabe, and G. Jackson, J. Phys. Chem. B **104,** 1322 (2000).
[28] C. McCabe, L. M. B. Dias, G. Jackson, and E. J. M. Filipe, Phys. Chem. Chem. Phys. **3,** 2852 (2001).
[29] L. X. Sun, H. G. Zhao, S. B. Kiselev, and C. McCabe, Fluid Phase Equilibria **228,** 275 (2005).
[30] L. X. Sun, H. G. Zhao, S. B. Kiselev, and C. McCabe, J. Phys. Chem. B **109,** 9047 (2005).
[31] C. McCabe, A. Galindo, A. Gil-Villegas, and G. Jackson, J. Phys. Chem. B **102,** 8060 (1998).
[32] R. P. Bonifacio, E. J. M. Filipe, C. McCabe, M. F. C. Gomes, and A. A. H. Padua, Molec. Phys. **100,** 2547 (2002).
[33] A. Galindo, S. J. Burton, G. Jackson, D. P. Visco, and D. A. Kofke, Molec. Phys. **100,** 2241 (2002).
[34] C. McCabe, A. Galindo, and P. T. Cummings, J. Phys. Chem. B **107,** 12307 (2003).
[35] A. Galindo, A. Gil-Villegas, P. J. Whitehead, G. Jackson, and A. N. Burgess, J. Phys. Chem. B **102,** 7632 (1998).
[36] F.J. Blas and A. Galindo, Fluid Phase Equilibria, 194–197, 501 (2002).
[37] A. Galindo and F. J. Blas, J. Phys. Chem. B **106,** 4503 (2002).
[38] C. M. Colina, A. Galindo, F. J. Blas, and K. E. Gubbins, Fluid Phase Equilibria **222,** 77 (2004).
[39] C. M. Colina and K. E. Gubbins, J. Phys. Chem. B **109,** 2899 (2005).
[40] A. Galindo, A. Gil-Villegas, G. Jackson, and A. N. Burgess, J. Phys. Chem. B **103,** 10272 (1999).
[41] A. Gil-Villegas, A. Galindo, and G. Jackson, Molec. Phys. **99,** 531 (2001).
[42] B. H. Patel, P. Paricaud, A. Galindo, and G. C. Maitland, Ind. Engng Chem. Res. **42,** 3809 (2003).
[43] M. D. Amos and G. Jackson, Molec. Phys. **74,** 191 (1991).
[44] M. Banaszak, C. K. Chen, and M. Radosz, Macromolecules **29,** 6481 (1996).
[45] F. J. Blas and L. F. Vega, Molec. Phys. **92,** 135 (1997).
[46] K. P. Shukla and W. G. Chapman, Molec. Phys. **91,** 1075 (1997).
[47] H. Adidharma and M. Radosz, Fluid Phase Equilibria **160,** 165 (1999).
[48] C. McCabe, A. Gil-Villegas, G. Jackson, and F. Del Rio, Molec. Phys. **97,** 551 (1999).
[49] F. Tumakaka, J. Gross, and G. Sadowski, Fluid Phase Equilibria, 194–197, 541 (2002).
[50] J. Gross, O. Spuhl, F. Tumakaka, and G. Sadowski, Ind. Engng Chem. Res. **42,** 1266 (2003).
[51] D. K. Singh and K. N. Khanna, J. Molec. Liquids **115,** 5 (2004).
[52] M. D. Amos and G. Jackson, J. Chem. Phys. **96,** 4604 (1992).
[53] R. P. Sear, M. D. Amos, and G. Jackson, Molec. Phys. **80,** 777 (1993).
[54] R. Dickman and C. K. Hall, J. Chem. Phys. **85,** 4108 (1986).
[55] R. Dickman and C. K. Hall, J. Chem. Phys. **89,** 3168 (1988).
[56] Y. C. Chiew, Molec. Phys. **70,** 129 (1990).
[57] Y. H. Song, S. M. Lambert, and J. M. Prausnitz, Macromolecules **27,** 441 (1994).
[58] S. H. Huang and M. Radosz, Ind. Engng Chem. Res. **29,** 2284 (1990).
[59] C. Pan and M. Radosz, Ind. Engng. Chem. Res. **37,** 3169 (1998).
[60] M. Banaszak and M. Radosz, Fluid Phase Equilibria **193,** 179 (2002).
[61] A. K. C. Chan, H. Adidharma, and M. Radosz, Ind. Engng Chem. Res. **39,** 4370 (2000).
[62] Y. P. Tang, Molec. Phys. **100,** 1033 (2002).
[63] J. Gross and G. Sadowski, Ind. Engng Chem. Res. **40,** 1244 (2001).
[64] J. Gross and G. Sadowski, Ind. Engng Chem. Res. **41,** 1084 (2002).
[65] J. S. Rowlinson and F. L. Swinton, *Liquids and Liquid Mixtures*, 3rd ed. (Butterworth Scientific, London, 1982).
[66] P. J. Leonard, D. Henderso, and J. A. Barker, Trans. Faraday Soc. **66,** 2439 (1970).
[67] T. Boublik, J. Chem. Phys. **53,** 471 (1970).
[68] G. A. Mansoori, N. F. Carnahan, K. E. Starling, and T. W. Leland, J. Chem. Phys. **54,** 1523 (1971).
[69] N. F. Carnahan and K. E. Starling, J. Chem. Phys. **51,** 635 (1969).
[70] H. S. Gulati and C. K. Hall, J. Chem. Phys. **108,** 7478 (1998).
[71] D. Frenkel and B. Smit, *Understanding Molecular Simulation: From Algorithms to Applications*, 2nd ed. (Academic Press, San Diego, 2001).
[72] C. McCabe and S. B. Kiselev, Ind. Engng Chem. Res. **43,** 2839 (2004).